

# EdgeLLM: A Highly Efficient CPU-FPGA Heterogeneous Edge Accelerator for Large Language Models

Mingqiang Huang, Ao Shen, Kai Li, Haoxiang Peng, Boyu Li, Hao Yu\*

**Abstract**—The rapid advancements in artificial intelligence (AI), particularly the Large Language Models (LLMs), have profoundly affected our daily work and communication forms. However, the colossal scale of LLM presents significant operational challenges, particularly when attempting to deploy them on resource-constrained edge devices such as smartphones, robots, and embedded systems. In this work, we proposed EdgeLLM, an efficient CPU-FPGA heterogeneous acceleration framework, to markedly enhance the computational efficiency of LLMs on edge. We first analyzed the whole operators within AI models and developed a universal data parallelism scheme, which is generic and can be adapted to any type of AI algorithm. Then, we developed fully-customized hardware operators according to the designated data formats. A multitude of optimization techniques have been integrated in the design, such as approximate FP16\*INT4 and FP16\*FP16 computation engines, group vector systolic arrays, log-scale structured sparsity, asynchronous between data transfer and processing. Finally, we proposed an end-to-end compilation scheme that can dynamically compile all of the operators and map the whole model on CPU-FPGA heterogeneous system. The design has been deployed on AMD Xilinx VCU128 FPGA, our accelerator achieves 1.67× higher throughput and 7.4× higher energy efficiency than the commercial GPU (NVIDIA A100-SXM4-80G) on ChatGLM2-6B, and shows 10%~20% better performance than state-of-the-art FPGA accelerator of FlightLLM in terms of HBM bandwidth utilization and LLM throughput.

**Index Terms**—Large Language Model, AI Accelerator

## I. INTRODUCTION

Artificial intelligence has captured keen interest and worldwide attention in the past ten years [1-5]. This is mainly associated with three pivotal advancements: First is the exponential escalation in computational prowess, which mainly attributable to GPU; Second is the evolution of AI algorithm [4-6], especially the convolutional neural networks for computer vision (CV), and the recurrent neural networks for natural language processing (NLP); Third is the AI big data [7,8], which serves as the foundational support for the training of AI models, fueling their precision and efficacy. These factors have coalesced to drive a transformative era in AI.

Since 2017, Transformer algorithm has rapidly become a dominant force in the field of artificial intelligence in terms of both NLP and CV research field [4-6]. By introducing the self-attention mechanism, Transformer altered traditional sequence modeling methods, no longer relying on recurrent neural networks (RNNs) or convolutional neural networks (CNNs) for feature extraction and sequence handling. This innovation not only enhanced the parallelization capabilities of models, making the training of large-scale models possible, but also significantly improved model efficiency and performance.

Following the success of Transformer, researchers began to explore even larger models, which typically have billions or more parameters, known as 'large language models' [9-11]. For example, the GPT (Generative Pre-trained Transformer) series of models from OpenAI, has showcased ability to understand and generate high-quality human language [11]. Nowadays, the large language models have begun integrating with other modalities such as vision and audio, showing capable of outstanding performance in cross-domain task. This interactive capability makes AI assistants, chatbots, and virtual agents more human-like and efficient [12-15]. In summary, large language models not only enhance AI's language processing capabilities but also advance broader technological progress in AI, bringing revolutionary changes to industries such as education, entertainment, healthcare, and business.

Nonetheless, the prevailing trend in contemporary AI accelerator architectures, especially those geared towards the demands of large language models, predominantly relies on the GPU paradigm. This conventional design, while powerful, exhibits inherent limitations that render it less than ideal for deployment on edge devices. The constraints imposed by the GPU architecture, such as high power consumption and extensive computational overhead, pose significant challenges to the practicality and efficiency of implementing AI capabilities at the network's periphery. Despite its attributes of high flexibility and high-performance capabilities in specific tasks, FPGA, a crucial component of heterogeneous computing, receives scant mention. The FPGA based implementation of LLM holds considerable promise for substantially enhancing computational efficiency and performance [16-20]. However, several critical challenges remain to be effectively addressed.

The first challenge within LLM is the vast diversity of operator types. Current AI chips grapple with the issue of non-uniform data formats for different operators, particularly when dealing with deep learning models. These models usually consist of a series of diverse operators: CNN networks predominantly utilize linear operations such as Matrix Multiplication, Convolution and Pooling operators [2]; while

---

This work was supported by STI 2030-Major Projects (2022ZD0210600), National Natural Science Foundation of China (NSFC) (Grant No. 62034007), Natural Science Foundation of Guangdong Province (Grant 2023B1515020051). (Corresponding author: Hao Yu)

Mingqiang Huang and Ao Shen contribute equally in this work.

Mingqiang Huang is with Shenzhen Institute of Advanced Technology, Chinese Academy of Sciences, Shenzhen 518055, China.

Ao Shen, Kai Li, Haoxiang Peng, Boyu Li and Hao Yu are with School of Microelectronics, Southern University of Science and Technology, Shenzhen 518055, China.(yuh3@sustech.edu.cn)

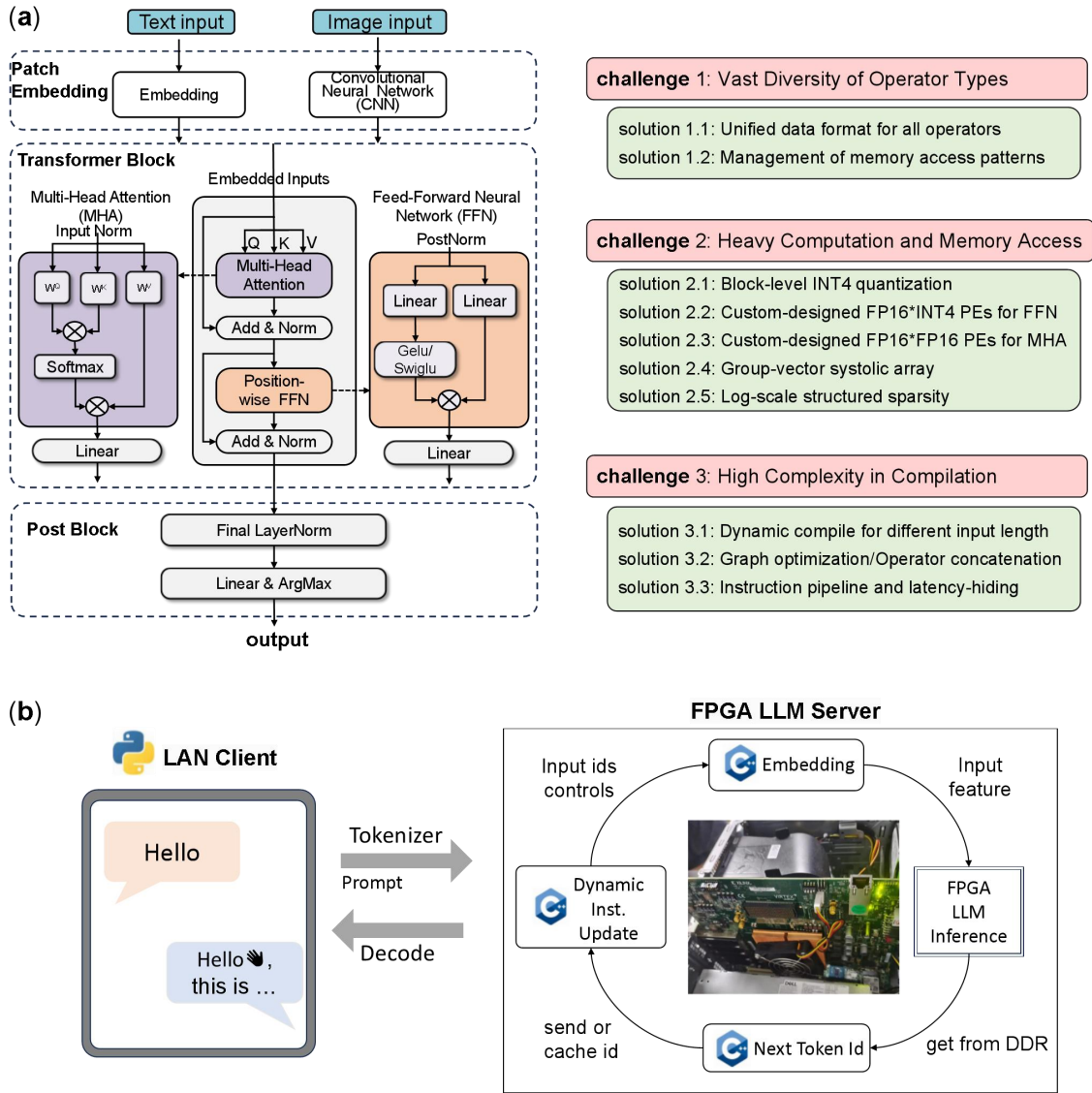


**Fig.1.** (a) Architecture of the Vision Transformer network and challenges in hardware design for Transformer-like accelerator. (b) Proposed CPU-FPGA heterogeneous acceleration system for the large language model.

the Transformer networks heavily rely on complex nonlinear operations such as Layer Normalization, multi-head Attention Mechanisms, Embedding Lookups and Positional Encoding [4,5]. Each operator potentially requires distinct data formats to achieve optimal computational efficiency. For instance, convolutional layers might prefer the NHWC format (batch size, height, width, channels) or the NCHW format (batch size, channels, height, width), while fully connected layers may be better suited to flat one-dimensional vector formats. In Transformer-like network, the diverse operators will bring more complex data format requirements. The absence of a standardized data format means that when data transitions from one operator to another, it often necessitates format transformations such as reshaping and matrix transposition. These additional operations not only add to the computational

load and consume precious computational resources but also introduce extra time lags, thereby reducing the overall system efficiency and throughput.

Another challenge is the massive parameter sizes and the resultant computational complexity [21, 22]. Large models, often boasting billions of parameters, require substantial computational resources during inference. This complexity arises from the intricate network architectures designed to capture nuanced patterns within large datasets, which in turn leads to higher accuracy in various AI tasks. The sheer volume of parameters translates into extensive memory requirements, making it difficult to fit these models into the memory of standard hardware. Moreover, the computational demands during inference can be prohibitive, as each operation across these parameters consumes considerable processing power and

time. To address such issue, several strategies have been developed, such as model pruning and quantization. As of now, INT4 quantization stands out as the most effective method for compressing large-scale models, offering significant improvements in computational efficiency and resource utilization [21]. In contrast, despite its theoretical advantages, sparse representation techniques have yet to gain widespread traction within the industry [23,24]. This discrepancy highlights the growing demand for hardware executing FP16\*INT4 operations, a capability that, notably, current generations of AI chips have not explicitly catered to through dedicated circuit design. As such, there exists a clear opportunity for innovation in the development of specialized hardware components tailored to the unique requirements of INT4 quantized models, poised to revolutionize the landscape of AI computation and deployment.

The final challenge lies within the compilation system, specifically addressing the vast number of operators and optimizing the linkage between them, which is crucial for enhancing computational speed [25]. In large models, the operator graph, which defines the computation flow, can be exceedingly complex with thousands of operators interconnected in intricate ways. Ensuring that the transition from one operator to another is seamless and efficient becomes a significant challenge. Traditional compilers are designed to optimize code for sequential execution, but the nature of deep learning models requires a different approach. The dataflow graphs of these models present opportunities for parallelism and pipelining that traditional compilers might not fully exploit. Therefore, specialized deep learning compilers and runtime systems have emerged to address these unique requirements. These compilers analyze the operator graph to identify opportunities for optimization, such as operator fusion, which combines adjacent operators into a single, more efficient operation. Another critical aspect is the management of memory access patterns. Efficiently handling the movement of data between different memory hierarchies can significantly impact performance. In summary, the compilation system for large models must be sophisticated enough to handle the complexity of the operator graph, optimize for parallelism, and manage memory access efficiently.

In this work, we develop an efficient CPU-FPGA heterogeneous acceleration system for large language model, where FPGA executes the core computational operators, and CPU executes the dynamic compilation process. When it comes to operational efficiency, our innovative design proposal outperforms both conventional GPU chips and state-of-the-art FPGA systems. This superior performance is achieved through a combination of optimized hardware architecture, efficient data handling mechanisms, and advanced dynamic compilation scheme. The contributions of our work are:

1. We have devised a unified and universal data format for the operator structures within AI algorithms, enabling the system to execute the entire sequence of operators swiftly and without interruption.

2. We have custom-designed dedicated FP16\*INT4 computational units, since INT4 quantization stands out as the most effective method for compressing large-scale models. Besides, we propose efficient FPGA computing engine with various optimizations including approximate computation, asynchronous communication, and group-vector systolic array for data processing. Moreover, we also proposed log-scale structured-sparsity computing engine to further boost the throughput.
3. We proposed end-to-end compilation scheme that can dynamically compile all of the operators and map the whole model on FPGA-CPU heterogeneous system.
4. The whole design has been successfully deployed on AMD Xilinx VCU128 FPGA platform. Our result achieves  $1.67\times$  higher throughput and  $7.4\times$  higher energy efficiency than GPU NVIDIA A100-SXM4-80G, and shows 20% higher performance than state-of-the-art FPGA accelerator of FlightLLM.

## II. BACKGROUND AND RELATED WORK

In this section, we will provide a concise overview about the algorithm of Transformers and Large Language Models, along with the advancements in high-performance LLM chips and the high efficiency FPGA based Transformer accelerator.

### A. Transformers and LLMs

Transformer model was first introduced in 2017 by the famous paper of "Attention is All You Need"[4], which broke through the limitations of traditional Recurrent Neural Networks (RNNs) and Convolutional Neural Networks (CNNs) when dealing with sequential data by adopting the self-attention mechanism. This mechanism allows the model to consider information from the entire sequence while processing any position within it, thereby theoretically achieving superior parallel processing capabilities and capturing long-range dependencies.

In 2018, the GPT (Generative Pre-trained Transformer) series of models from OpenAI, has showcased the enormous potential of language models in generation and understanding. GPT-3, in particular, is noteworthy with its 175 billion parameters, demonstrating an ability to understand and generate high-quality human language [11]. In 2019, a research team from Google introduced the Text-to-Text Transfer Transformer (T5), a unifying framework that reformulates virtually all natural language processing (NLP) tasks as text-to-text transformation problems [26]. Through pre-training and fine-tuning, T5 demonstrated outstanding performance across a spectrum of NLP tasks, further validating the flexibility and robust adaptability of the Transformer architecture [27].

As research progressed, the Transformer architecture began to be applied to multimodal tasks, such as image captioning and video understanding, achieving effective integration of cross-modal information. The famous models include GPT Series [11], ChatGLM [28], PaLM [29], Sora [30] and so on. These large models demonstrate remarkable abilities in their respective fields, ranging from simple text generation to

complex multi-modal understanding and generation, continuously pushing the boundaries of artificial intelligence technology. As technology advances, we anticipate that more innovative large models will emerge, bringing about even more intelligent applications and services.

### B. AI Chips for Transformers and LLMs

AI chips that support the operation of large language models typically require high computational power, high memory bandwidth, and an efficient parallel processing architecture. So far, most of current AI accelerator systems, particularly those for large language models, are exclusively based on CPU-GPU architecture, such as NVIDIA's A100 GPU, Google's TPU [31, 32], Intel's Habana Gaudi AI training processor, Graphcore's Intelligent Processing Unit (IPU), and AMD's Instinct MI200 series GPU. These AI chips usually provide abundant computational resources ( $> 100$  TOP/s), high memory bandwidth ( $>1$  TB/s), and optimized parallel processing capabilities, effectively supporting the training and inference of large-scale models, meeting the demand for computational power in modern AI applications.

To catalyze the pervasive integration of AI across societal and industrial landscapes, a critical imperative emerges: the necessity for AI's seamless deployment on a diverse spectrum of edge-side hardware, transcending the confines of cloud-based accessibility. FPGA implementation offers flexibility in design, allowing for customization and optimization of the model for specific applications, thus is particularly suitable for the edge application. Currently, there have been several advances in such fields.

The work of [33] maps a 172 GFLOP Neural Machine Translation model with mixed-precision representation to a single FPGA board, which is the first work on implementation a real-life end-to-end NMT model to FPGA. But the work is operated on low frequency of 100MHz and shows relative low throughput. [34] proposes the ViA, a novel vision Transformer accelerator architecture based on FPGA, to execute the transformer application efficiently. They obtained nearly 309.6 GOP/s computing performance in the peek on FP16 data type. [20] propose an integer-only accelerator for Transformer, and the average throughput reaches as high as 762.7 GOPs, demonstrating significant acceleration performance improvement compared to previous state-of-the-art accelerators. But the integer model is not suitable for the large language model.

FlightLLM [16] is the first FPGA based LLM accelerator, by introducing configurable sparse digital signal processor (DSP) chain for various sparsity patterns, and always-on-chip decode scheme with mixed-precision support to enhance memory bandwidth utilization. FlightLLM achieves  $6.0\times$  higher energy efficiency and  $1.8\times$  better cost efficiency than the NVIDIA V100S GPU for Llama2-7B models, with  $1.2\times$  higher throughput than the NVIDIA A100 GPU during decoding, showing great potential for the FPGA based LLM acceleration system. However, the bandwidth utilization is 65.9%, which is still not that high and can be further improved.

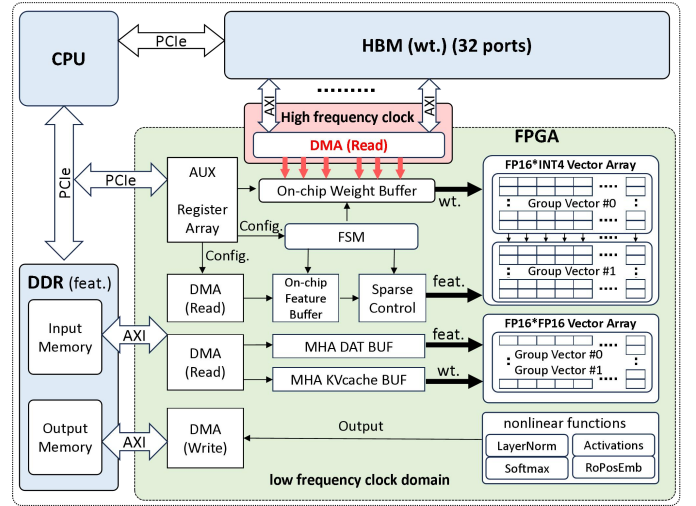


Fig.2. Overall architecture of the LLM accelerator proposed in this work.

## III. COMPUTING ARCHITECTURE

In this section, we will overview the basic architecture of accelerators, analyze the operators in various neural network models, and discuss the problems related to data formats.

### A. Overall Architecture

Fig. 2(a) provides the basic architectural diagram of the proposed CPU-FPGA Heterogeneous accelerator. The system contains four elements: the Central Processing Unit (CPU), High Bandwidth Memory (HBM), DDR memory and the LLM Accelerator. The CPU acts as the brain of the system, interfacing with the remaining components via the Peripheral Component Interconnect Express (PCIe) bus. It wields direct access privileges over DDR and HBM through the AXI-full protocol, enabling both read and write operations. Furthermore, it leverages the AXI lite protocol to interact with the accelerator IP's internal register array, thereby exercising control over the accelerator's operational dynamics. Within the accelerator IP, all of the operators have been meticulously incorporated, including matrix multiplication operator, multi-head attention mechanisms operator and so on. Among these, matrix multiplication operator, due to its extremely high demand for handling vast quantities of parameters, is connected with the High Bandwidth Memory (HBM). The other operators engage in data transactions with the Double Data Rate (DDR) memory, illustrating a differentiated memory access strategy tailored to the specific requirements of each operator.

When accelerating the LLM models, all of the weight parameters (using INT4 quantization method) will be pre-processed and stored in HBM, whereas the dynamically generated activation data is consigned to DDR. Within the accelerator IP, all of the operators are specifically designed with customized Direct Memory Access (DMA) modules, tasked with fetching activation data between out-chip DDR and on Block Random Access Memory (BRAM) caches.

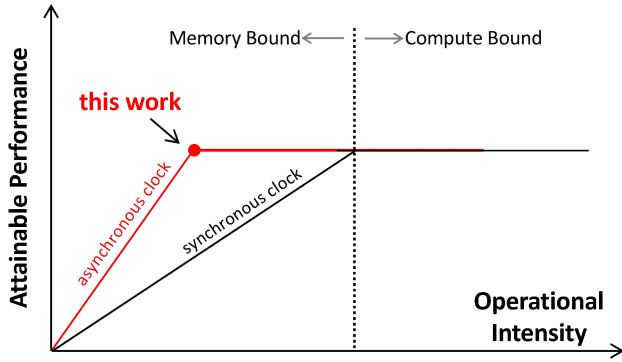


Fig.3. Roofline model and the designed operation point of this work.

Figure 3 shows the roofline model [35] when accelerating the matrix multiplication (MatMUL) operator, serving as a pivotal analytical tool to contrast the boundaries of memory-limited and computation-limited domains. This graphic representation illuminates the performance characteristics of MatMUL operator under both synchronous and asynchronous clocking regimes. The operational intensity, quantified as the ratio of teraflops per byte (TFLOP/Bytes), spans the horizontal axis, whereas the vertical axis delineates the achievable performance, measured in teraflops per second (TFLOP/s). The roofline model adeptly demarcates the shift from memory-bound to compute-bound scenarios, with the black line tracing the performance trajectory of MVM under synchronous clock conditions, and the red line charting the same under asynchronous clocking. This visual juxtaposition offers profound insights into how varying clocking strategies influence the operational intensity and attainable performance of MVM, thereby elucidating the intricate interplay between memory bandwidth and computational throughput.

To harness the high-speed communication prowess of HBM, we have engineered a computation array that aligns impeccably with the roofline model. In the specific task of LLM operating with a KV cache framework, the matrix-matrix multiplication (MatMUL) task can be simplified into vector-matrix multiplication (MVM). Here in our system, the HBM's bandwidth is 8192 bits per cycle (32 AXI ports, and each port transmits 256 bits per cycle). To full utilize this high bandwidth, we set the system to consume a corresponding 8192 bits of weight parameters per cycle, which means a system computational parallelism of 2048 (under INT4 quantization scheme). Furthermore, we have doubled the computation parallelism up to 4096 to further increase the throughput, meanwhile the HBM-AXI communication module and DMA module will operate at a twice higher frequency than that of the computational module, which has been shown in fig.3 (red dot).

### B. Unified Data Format

The traditional CNN networks are predominantly utilizing linear operations such as Matrix Multiplication, Convolution and Pooling. However, the Transformer networks heavily rely

on complex nonlinear operations such as Attention Mechanisms, Layer Normalization, Embedding Lookups and Positional Encoding [4-6]. When executing an artificial intelligence model, the compilation process of the system relies on the operator graph to achieve coherence and efficiency. The operator graph, essentially a directed acyclic graph (DAG), represents the computation flow of the model, where nodes correspond to individual operators or operations, and edges denote the data flow between these operators. Ensuring that each operator's inputs and outputs maintain a consistent data structure is paramount to achieving optimal execution speed and minimizing runtime errors. This consistency allows for smooth transitions from one operator to the next, as each operator expects a specific type of input and produces a corresponding output. When these data structures align, it facilitates a seamless flow of data throughout the model, enabling the system to execute the entire sequence of operators swiftly and without interruption.

In this work, we developed a universal data parallelism scheme after carefully analyzing the whole operators within AI models. The scheme is generic and can be adapted to any type of AI algorithm. As shown in fig.4a, the text-type input/output activation data innately embodies a two-dimensional structure of (tokens, channels). The data can be easily transformed into three-dimensional tensor representation, namely  $[CH/T_{out}, token, T_{out}]$ . Here,  $T_{out}$  represents the parallelism degree in data channel direction. Similarly, the image-type input/output activation data (fig.4b), which is originally characterized by height (H), width (W), and channels (CH) can be transformed into four-dimensional tensor representation of  $[CH/T_{out}, H, W, T_{out}]$ . It can be seen that, the text-type and image-type data are sharing with the same tensorization scheme. Such unification not only streamlines data handling but also underscores the inherent compatibility and adaptability of tensor representations across diverse data modalities. Moreover, this architectural framework effortlessly scales to accommodate the intricacies of more complex data types. In scenarios where multi-head attention mechanisms introduce an additional head dimension, or during batch processing where a batch dimension is appended, the data dimensions can be expanded analogously as  $[head, CH/T_{out}, H, W, T_{out}]$  or  $[Batch, CH/T_{out}, H, W, T_{out}]$ , ensuring that the framework remains versatile.

Another advantage of such data format lies in the universal applicability across all operator types, coupled with the maximization of efficiency in leveraging AXI burst transfers. The term "burst transfer" refers to the ability of the interface to transfer multiple consecutive data words in a single transaction, rather than initiating a new transaction for each word. In our design, the data-width in both AXI write-mode and AXI read-mode is fixed at  $T_{out} * 16$ , which is just the same as the smallest data package in  $[Batch, CH/T_{out}, H, W, T_{out}]$ . Therefore, the incremental address in AXI burst transfer will exactly be the W-index in the tensor. This allows for efficient sequential data access, making it particularly useful for reading or writing blocks of data in memory.



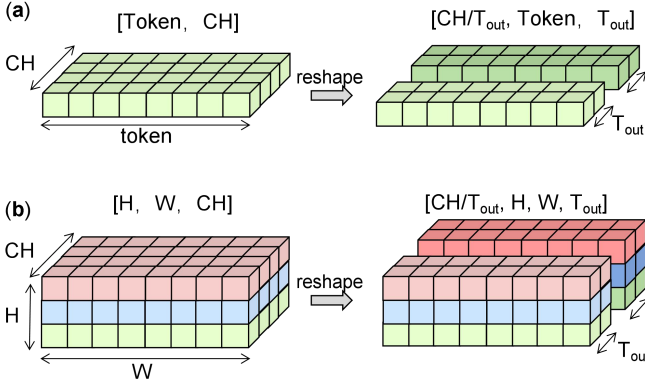


Fig.4. Data package method in the accelerator.

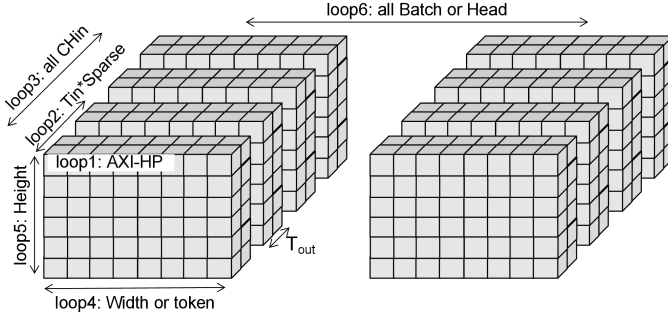


Fig.5. Customized data access method and the Direct Memory Access (DMA) loops.

Figure 5 depicts the DMA (Direct Memory Access) system designed for our matrix-multiplication operator, which employs a hierarchical approach focused on optimizing data handling and sparsity management through AXI burst transfer protocol. As the highest tier, Loop-1 manages continuous address increments along the width axis of the feature data, ensuring successive data transfers aligned with the AXI protocol. Subsequently, Loop-2 ( $T_{in}$  Loop) plays a critical role in for the hardware systolic PE array, which requires input channel depth of  $T_{in}$  for input features, and output channel depth of  $T_{out}$  for output feature, namely the total parallelism is  $T_{in} \times T_{out}$  ( $128 \times 32$ ). The further loop is designed to fulfill the sparsity levels by transmitting  $T_{in} \times \text{current\_sparsity}$  along the input channel depth direction, enabling the selection of feature data with different sparsity patterns. Loop-3 ( $CH_{in}$  Loop) ensures the accumulation of all input channel depths before computing the final matrix-multiplication results, minimizing unnecessary on-chip data storage and enhancing overall system efficiency. The Width-Loop (Loop-4) and Height-Loop (Loop-5) hold lower priority and are activated once output feature pixel computations commence. The last loop (Loop-6) is for different head or batch feature data. These loops manage traversals across the spatial dimensions of the data matrix, ensuring no delays in handling output data. The output DMA configuration, though simpler, mirrors the input approach by employing loops for continuous address increments along the output feature width and other loops to manage output

dimensions, securing an orderly transmission of computed features from on-chip to off-chip storage. Such design not only meets the high computational demands of matrix-multiplication operations but also streamlines data flow efficiency, making it an integral component in optimizing the performance of our accelerators.

#### IV. HARDWARE DESIGN

This section discusses hardware design and optimization strategies for the matrix multiplication operator and multi-head attention operator, including group vector systolic array, approximate computing, sparse coding, and operator fusion in multi-head attention.

##### A. Design Methodology for Matrix Multiplication Operator

Large language models (LLMs) often contain billions of parameters. This massive size presents significant challenges in terms of storage, memory, and computational efficiency, especially when deploying these models on devices with limited resources or when attempting to scale up distributed training processes. INT4 quantization, which represents weights using 4-bit integers instead of the typical 32-bit or 16-bit floating-point numbers, offers several advantages: higher memory efficiency, higher computation speed and better bandwidth optimization, thus has been widely used in the inference of LLM. To improve the computation efficiency, we utilized both grouped vector systolic array and approximate computing strategies.

When addressing the regulation of the computational array, it becomes imperative to consider various facets including synchronization, data flow management, and optimization techniques to ensure the array operates at peak efficiency and reliability. In our previous research endeavors, we had conceptualized and developed the grouped vector systolic computing array, a pioneering architectural innovation geared towards realizing highly efficient and parallel computation [19]. This design was centered around leveraging vector processing principles within a systolic array framework, thereby enabling the execution of complex computational tasks with remarkable speed and energy efficiency, particularly suited for large-scale data processing and intensive numerical computations.

Furthermore, we have designed an efficient and highly accurate FLOAT\*INT multiply-accumulate (MAC) unit, which consists four-stage data flow as shown in figure 6. The  $FP16 \times INT4$  MAC array module can support  $T_{in}$  number of FP16 (feature data) and INT4 (weight data) inputs for vector-multiplication, in which  $T_{in}$  is the vector length and can be set as 16/32/64/128/256. To align with the computational requirements of the block-level INT4 quantization algorithm, the unit also supports the multiplier of Scale value (in FP16 data-type) to adjust the final output. In Stage-0, the FP16 will be split into sign bit (S), exponent bit (E), and mantissa bit (M), while INT4 data will be split into sign bit (S) and mantissa bit (M).

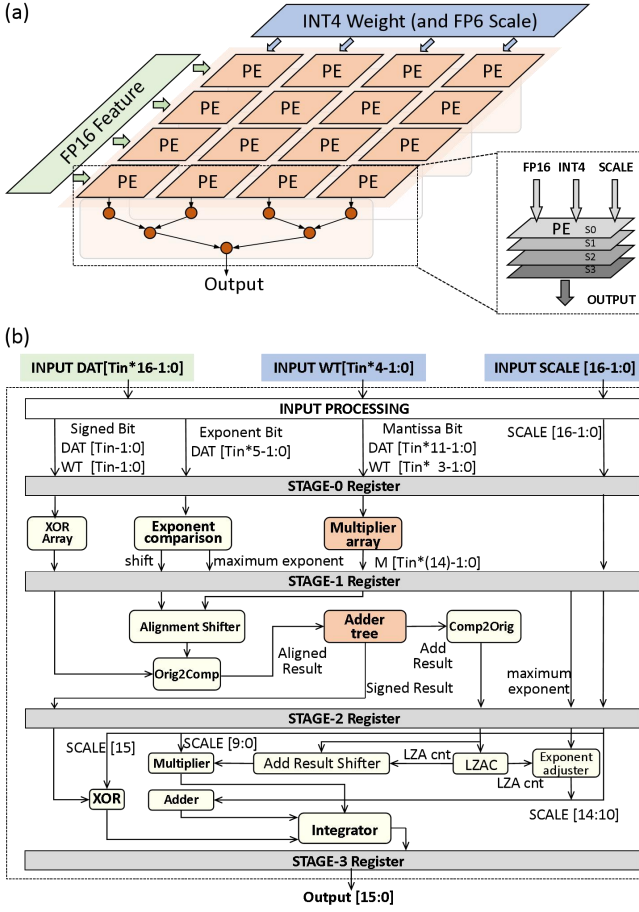


**Fig.6.** (a) Group vector systolic array. (b) Architecture of the fully customized FP16\*INT4 vector multiplier.

In Stage-1, an exclusive-or (XOR) operation is performed between the sign bits of each FP16 DAT and the INT4 WT. Concurrently, the exponent bits of FP16 data are analyzed by the exponent comparison module, which identifies the highest values among all FP16 inputs. The module computes the exponent distance between each input and the maximum one. Meanwhile, the mantissa bits of FP16 and INT4 will be sent to the multiplier array for a multiplication operation. Within the multipliers, a deliberate design choice has been to preserve the entirety of the mantissa components. This meticulous approach serves to significantly retain the precision of our computational outcomes, ensuring that no fractional detail is lost in the arithmetic processes.

In Stage-2, the exponent distances and the multiplication results obtained in Stage-1 will be fed into the alignment shifter module for aligning the decimal points. Then the shifted mantissa results will be sent into the adder tree module for accumulation. Recognizing that the preliminary shifting operations, the input data width will be increased. To avoid excessive resource consumption, we have specified the bit-width of the adder tree as 19 bits, resulting a balance between resource utilization and computational accuracy.

**TABLE I. Comparison of the different FP16\*INT4 unit**

@Tin = 128		this work	baseline1	baseline2
<b>computation error</b>		0.04718%	2.86372%	2.64440%
<b>ASIC flow</b>	Total Area	67075 um2	80675 um2	110668 um2
	Total Power	41.74 mW	35.03 mW	41.58 mW
	Maximum Frequency	1.69 GHz	1.03 GHz	1.06 GHz
<b>FPGA flow</b>	LUT	30346	24060	37320
	FF	12348	4151	4596
	DSP	0	128	128

**TABLE II. Comparison of our FP16\*INT4 module at different input vector length**

FP16*INT4 PE		Tin 32	Tin 64	Tin 128	Tin 256
<b>computation error</b>		0.04240%	0.04440%	0.04718%	0.04997%
<b>ASIC flow</b>	Total cell area	15819 um2	32664 um2	67075 um2	131047 um2
	Total Power	10.609 mW	20.846 mW	41.745 mW	86.762 mW
	maximum Frequency	1.89 GHz	1.82 GHz	1.69 GHz	1.64 GHz
<b>FPGA flow</b>	LUT	6811	13810	30346	54916
	FF	3102	6184	12348	21300
	DSP	0	0	0	0

In Stage-3, the multiplication result and maximum exponent obtained from the previous layers will be converted into specification FP16 data through LZA (Leading Zero Anticipate) module and exponent adjustment module. Then they will be multiplied with the initial input of Scale value and get the final result using floating point multiplication. Finally the result will be inputted into the integration module to be adjusted into FP16 for output.

To validate the efficiency of our proposed scheme, we design two additional sets of control experiments. In these experiments, a standard pairwise addition-based adder tree was employed; however, the precision of intermediate calculations varied. In one case, we configured the intermediate temporary results to be represented in the FP16 format. Conversely, in another case, a customized FP20 data format is used to avoid overflows during computing, meanwhile maintaining high accuracy due to the large bit width of mantissa. Note, we set the sign bit width to be 1, exponent bit width to be 6, and the mantissa bit width to be 13 in FP20 data type.

Performance comparison of the different FP16\*INT4 unit design methods have been shown in Table 1. The proposed FP16\*INT4 module exhibits significantly lower computational errors when compared with the two baseline schemes. Under

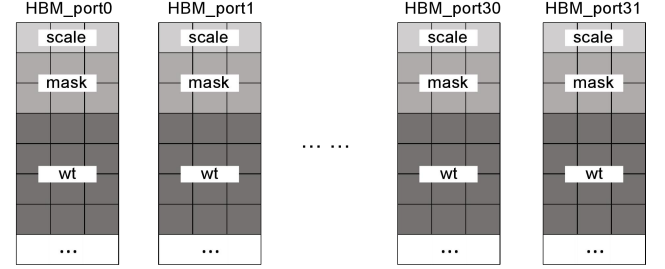
100,000 random input tests, our methodology manifests a mere 0.047% error rate. While the baseline method of 1 and 2 incur error rates exceeding 2.5%. The disparity primarily attributed to the substantial truncation errors incurred during the S1 phase. This marked discrepancy underscores the superiority of our design approach. Besides, our design exhibits the highest comprehensive performance in terms of Power, Performance, and Area (PPA). Firstly, the design shows 16.85% area reductions when compared with Baseline 1 and 39.39%-decrease with Baseline 2. Secondly, our module outperforms competitors in clock frequency, achieving a peak of 1.69GHz on a 28nm CMOS, approximately 1.6 times higher than that of Baselines 1 and 2. Lastly, concerning power consumption, Baseline 1, due to its inherently lower computational complexity in FP16 operations, naturally incurs the least power draw. Nevertheless, our scheme exhibits a mere 20% increment in power consumption, demonstrating commendable efficiency. These attributes confirm our approach as the optimal PPA performer.

Next, we compare our FP16\*INT4 module at different input vector length ( $T_{in}$ ) as shown in Table 2. The maximum frequency slightly decreases as vector length increasing. The circuit area and consumption scales almost linearly with  $T_{in}$ , aligning perfectly with theoretical expectations. This finding further consolidates the robustness and scalability of our design across diverse operational scenarios.

### B. Optimization for Matrix Multiplication Operator

Structured sparsity offers significant advantages. It boosts computational speed by skipping zero weights, reduces storage needs for large models, saves energy, and enables complex models to run on devices with limited resources, all while maintaining accuracy. Density bound block (DBB) based structured sparsity have proven to be an effective method, but it is still an open question to explore which kind of structure sparse is the best. Previous work [36] focused on the linear distribution of sparsity (namely 1/8, 2/8, 3/8...), but the hardware utilization is usually low, resulting in low efficiency. The GPU [37] based fix sparsity (2/4 weight sparsity) shows high efficiency, but it get only  $2\times$  throughput speedup. To overcome the above challenges, this paper presents log-scale structured-sparse (namely 1/2, 1/4, 1/8...) accelerator. With the help of time-unrolled micro-architecture, the hardware utilization can reach 100% in a wide range of sparsity when compared with the linear one.

We utilize structural sparsity into the weight parameters in the matrix multiplication operator. During the execution of matrix multiplication, a broader range of activation data is initially fed into the system. Subsequently, the necessary activation data is selectively picked out based on the mask within the weight parameters. Finally, both the selected activation data and the weight data are jointly directed into the computational array for processing. An efficient sparse DMA has been designed for the feature data (see section III).



log-scale structured sparse		case1: dense	case2: 50% sparse	case3: 75% sparse	case4: 87.5% sparse
scale	effective block size	128	64	32	16
	CH in one group	2048	2048	2048	2048
group nums		16	8	4	2
mask	CH in one group	0	256	512	1024
	row in one group	0	1	2	4
wt	row in one group	2	2	2	2
Total rows for CH=2048		$1+16*2 = 33$	$1+8*(1+2) = 25$	$1+4*(2+2) = 17$	$1+2*(4+2) = 13$
effective Bit-width		4.125 bit	3.125 bit	2.125 bit	1.625 bit
Performance Enhancement		-	1.32 $\times$	1.94 $\times$	2.54 $\times$

Fig.7. Analysis on the effective weight bit-width and performance enhancement at different log-scale mix sparsity.

For the weight data, block quantization [21,22] and hybrid sparsity schemes are used, wherein 128 adjacent parameters are symmetrically quantized and share the same quantization scale parameter. The log-scale mix sparsity is defined as that every group of eight adjacent data blocks must contain at least N zeros (and 8-N are non-zeros). For example, when the sparsity is 75%, it means each eight adjacent data blocks must contain at least 6 zeros and at most 2 non-zeros. Based on these analysis, the parameters can be categorized into three types: quantization scales, masks, and the weights themselves, all of which will be stored in HBM.

Given that the single HBM AXI-port in this FPGA has an bit width of 256 bits, and each quantization scale is in FP16 datatype, the group size will be  $256/16 * 128 = 2048$  input channel groups ( $CH_{in}$ ).

case1: when the model is dense, the 2048  $CH_{in}$  groups contain a total of  $2048 * 4 = 8192$  bits of INT4 weights. Since each row of HBM has a bit width of 256 bits, it requires  $8192 / 256 = 32$  rows.

case2: when the layer sparsity of the model is 50%, the mask requires 8 bits, while the weight (WT) data requires  $8*50\%*4=16$  bits. Consequently, for these 2048 CH groups, the weight parameters require 16 rows of WT and 8 rows of masks.

case3: when the layer sparsity of the model is 75%, the mask requires 8 bits, while the weight (WT) data requires  $8*25\%*4 = 8$  bits. Consequently, for these 2048 CH groups, the weight parameters require 8 rows of WT and 8 rows of masks.



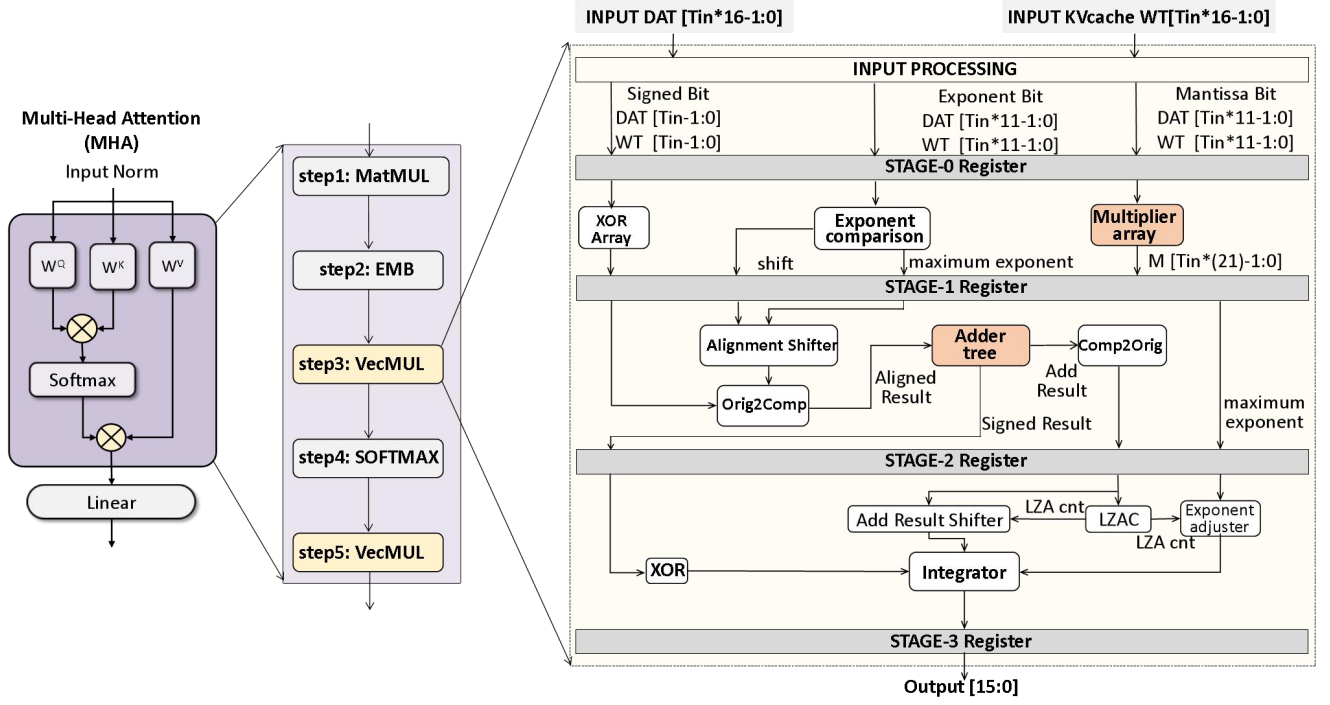


Fig. 8. Structure of multi-head self-attention (MHA) block, which contains matrix multiplication, rotary position embedding, multi-head matrix reshape, vector matrix multiplication, Softmax and so on. The core operation of vector matrix multiplication is performed in the optimized FP16\*FP16 module.

case4: when the layer sparsity of the model is 87.5%, the mask requires 8 bits, while the weight (WT) data requires  $8 \times 12.5\% \times 4 = 4$  bits. Therefore, the weight parameters require 4 rows of WT and 8 rows of masks.

According to the above analysis, the effective wt bit-width is 4.125bit, 3.125bit, 2.125bit, and 1.625bit, respectively. And the performance enhancement ratio will be 1.32 $\times$ , 1.94 $\times$ , 2.54 $\times$  for different sparsity.

### C. Design Methodology for Multi-Head Attention Operator

Multi-head self-attention (MHA) is considered to be the key innovation for Transformer [4]. But the original MHA is too complex and contains more than 10 step of different operators. Take the ChatGLM2 model as an example (Fig.8). The shape of the input activation is (token, 4096), and weight matrix of  $W_q$  is (4096, 4096), of  $W_k$  and  $W_v$  is (4096, 256). After the matrix multiplication, we will get the three matrixes of Query-Key-Value in (token, 4096), (token, 256), (token, 256), respectively. In the multi-head self-attention mechanism, the Query-Key-Value matrix will be further embedded and reshaped according to the head numbers, generating a three-dimensional matrix of (head, token, 4096/head). Next, the context information will be calculated by  $Q \cdot K^T$ , in which  $Q$  is the Query matrix,  $K^T$  is the transpose of Key matrix. It should be noted that  $K$  is generated by the former matrix multiplication of  $INPUT \cdot W_k$ , therefore  $K^T$  is also generated on-line and can not be pre-treated during the inference process.

The attention matrix will be performed by Softmax and finally multiplied by the Value matrix. Given that  $Q$ ,  $K$ , and  $V$  represent high-dimensional tensors, the aforementioned function inherently entails irregular and non-contiguous memory access patterns. Intuitively, edge deployment of complex operations involving such tensor data is arduous, owing to the resource limitations typical of edge devices.

To simplify the aforementioned computations, we have devised a novel attention mechanism operator articulated through a five-step methodology as shown in Fig.8. Among these alterations, the paramount characteristic is that, ensuring each operator's inputs and outputs maintain a consistent data structure as discussed in section III. For the Softmax function, the quintessential requirement is to facilitate concurrent computation for two distinct modes: the prefill scenario incorporating masked inputs, and the decode configuration featuring unmasked inputs. For the VecMUL operation, a salient point to consider is that the weight parameter of  $K^T$  and  $V$  are both generated on-line and formatted in FP16. This necessitates the creation of a specialized vector computation operator tailored for FP16\*FP16 operations. Here we adopt the similar design methodology as discussed in Fig.6. Additionally, it is worth mentioning that the KV-cache plays a pivotal role in optimizing performance and resource management. Designed to store key-value pairs, this cache mechanism significantly enhances computational efficiency by enabling rapid retrieval of previously computed values, thereby reducing redundant calculations and minimizing latency.

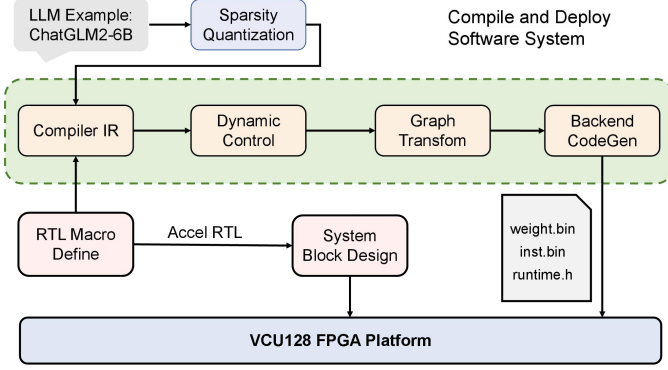


Fig. 9. Compilation and deployment of LLM on VCU128 FPGA platform.

## V. SOFTWARE DESIGN

In this section, we will introduce the software design and compilation strategies aimed at optimally invoking the hardware operators detailed above.

### A. Software Architecture and Inference Systems

In addition to the hardware design, this work also proposes software design and optimization on the deployment of LLM. Figure 9 shows the compilation and deployment of LLM on VCU128 FPGA platform using ChatGLM2-6B as an example. After sparse and quantized, the LLM will be imported into the compiler, and the compiler will do special optimization of the LLM including dynamic control and KV-cache, and finally generate instructions, pre-processing weights and runtime control code according to the characteristics of the accelerator to facilitate model deployment. According to the compiled model, we designed a set of LLM inference framework based on LAN (local area network). It uses FPGA and the deployed LLM as the server side, which is responsible for the actual inference of the LLM. Python is used to act as the client to encode and decode the token ids, and conducting direct interaction with users. Before the practical testing, it's imperative to assemble and organize the weight parameters as discussed in section III. Furthermore, the appropriate configuration data for the operator registers needs to be meticulously prepared, ensuring that all components are correctly initialized for the upcoming testing phase.

### B. Dynamic Compile Scheme

The compilation of large models faces a variety of challenges, which mainly stem from the scale, complexity, and real-time requirements of the models. Moreover, In the inference process of the LLM, the shape of the data input is constantly changing according to the actual input or generated tokens. In most cases, the compiler can only make the optimal optimization for the corresponding hardware inference platform under the static model, therefore the compiler's support for dynamic shape is almost insufficient, and some even need to compile the static model for all input cases, which will obviously waste a lot of storage space for instruction storage.

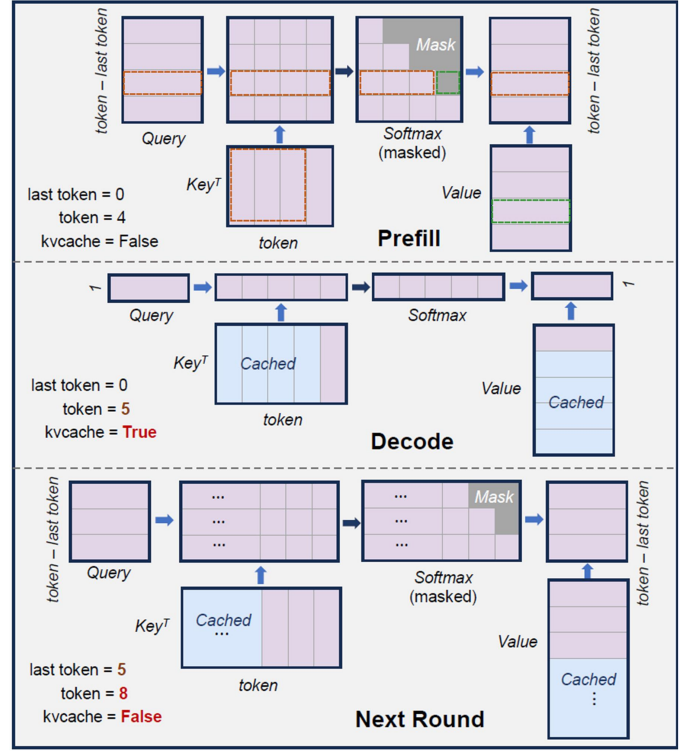


Fig. 10. Dynamic compile scheme for both prefill (Question) and decode (Answer) inference of the LLM.

In this design, for the LLM inference problem of the dynamic shape, we consider that the dimension of the input data will not change, but the number of tokens will change according to the inference situation. Therefore, it is possible to convert the dynamic token parameters into a static state as much as possible. First of all, in order to simplify the dynamic addresses for all operator outputs, the compiler introduces the MAX Token attribute from RTL Macro Define. It replaces the dynamic token in the calculation of the memory space size and address of dynamic data to make the address static, reducing a lot of additional computation caused by the dynamic change of addresses at runtime. Second, hardware instructions also need to adapt to dynamic token. When the compiler evaluates the hardware instructions for the corresponding operator, the token is involved as a Variable and the parameters are recorded as numeric expressions in the form of Directed Acyclic Graph (DAG). If this parameter can be evaluated directly, the compiler returns the result of this instruction, otherwise it is embedded in the runtime code in the form of a simplified code expression for real-time updates. In this approach, the hardware instructions require very little space, making the inference space of KV-cache very sufficient. This design supports up to 16k token generation.

In order to minimize the number of instructions that need to be dynamically updated, according to the characteristics of KV-cache inference of the LLM, we introduce two additional control parameters, *kvcache* (bool) and *last token* (int), in addition to *token* (int), as shown in Fig. 10.

KV-cache inference is mainly divided into two stages, prefill and decode. In the prefill phase, *kvcache* is set to false, *token* that will participate in the instruction configuration as the actual input data dimension. In the decode phase, that is, when *kvcache* is true, the dynamic control will fix the dimension of the input data to 1, and *token* will record the number of token generated instead of the corresponding data dimension to calculate the address offset when needed. During the inference of multiple rounds of Q & A, the *last token* parameter will be enabled to record the length of the cache data during the last round of Q & A and re-update the base address of the prefill phase. According to this setting, except that the instructions need to be fully updated in the prefill phase, only a small part of the parameters need to be updated in the decode phase, which greatly reduces the delay needed to update the parameters.

### C. Operator Concatenation and Graph Optimization

Another difficulty in dynamically compiling large models is the Memory Management. Large models often need to handle massive intermediate computational results and parameters, which can lead to inefficient memory usage and fragmentation issues. Besides, large models typically contain complex computational graphs that may include redundant operations or ineffective paths. The compiler needs to be able to identify and eliminate these redundancies while applying various optimization techniques.

For each operator in LLM, it is necessary to correctly connect its corresponding inputs and outputs, and carry out reasonable optimization according to the situation of the model graph, and finally allocate space and address for each node, so that the series of the entire accelerator operator becomes effective. Operator fusion as a common optimization method, accelerator and compiler also supports many operator fusion methods, such as MVM and Batch Norm operation, transpose and MatMul operator fusion, Add Mask and Softmax operator fusion and so on. The compiler implements the conversion and fusion of the operators of the computed graph, and in the case of ChatGLM2-6B, the one block in model will be fused into 14 hardware operations as shown in Fig. 11.

In LLM inference, the results of *k* and *v* need to be continuously cached and concatenated with newly generated *k* and *v*. Therefore, we added the optimization of KV-cache in the process of graph transformation. According to the MAX Token parameter, the compiler converts the data that needs to be cached into the data of [Head, CH//T<sub>out</sub>, MAX Token, T<sub>out</sub>]. Then the base address of the data is adjusted according to the token parameters of the runtime, and the data is offset in the form of T<sub>out</sub>\*token\*sizeof(float16). On this basis, when the compiler plans memory, it focuses on dividing inference time memory into two types, the regular runtime type and the cache type. The Runtime type takes maximum utilization into account, so it is constantly overridden in the form of Ping-Pong. The cache type guarantees that no other operator's results will be written at any time. With this, we have completed the support and optimization of KV-cache mode.

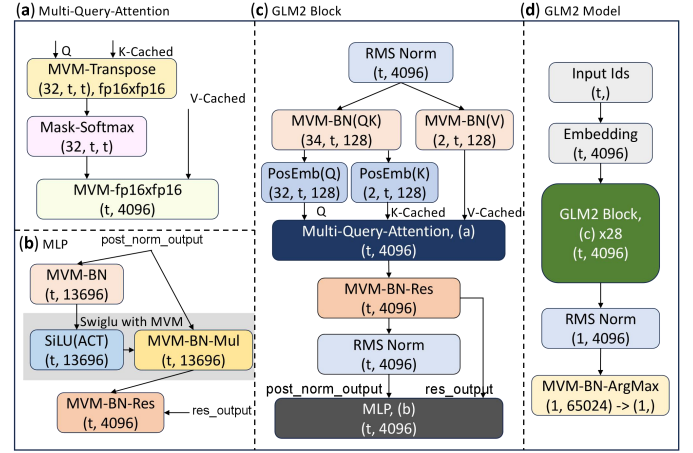


Fig. 11. Optimized operator graph.

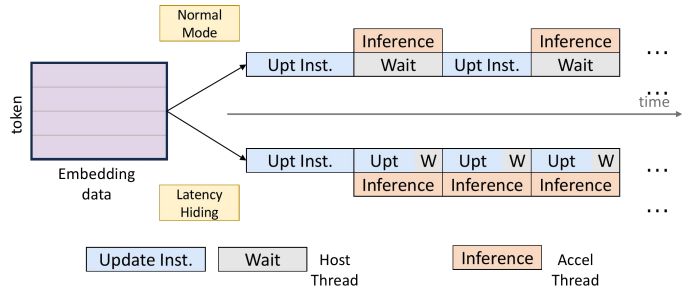


Fig. 12. Optimization of latency hiding in the inference stage.

In addition, since the effective data of all operators after the last attention structure is only on the vector of the last token, and the remaining tokens are redundant calculations, the compiler makes additional optimization on this, and gives the actual data offset according to the token parameter. The data of the last token is removed for subsequent calculations to minimize the amount of computation.

Besides, our design provides AUX mode with auxiliary path to realize the mode operation of instruction pipeline, the compiler can provide the optimization of delay hiding in the inference stage, as shown in the Fig. 12. The accelerator AUX mode can encode multiple serialized operator instructions directly from the on-chip DDR to the buffer via the AXI bus. In the host control of the accelerator, only the configuration information of the given serialization instruction needs to be written to the register, such as the address information, the number of valid operators, etc. The accelerator will then complete the rapid start and continuous operation of the serialization instructions. After the accelerator reads the instructions, the host has additional time to perform other calculations before completing the accelerator calculation. Thus, the delay required for dynamic control instruction updates can be hidden in the time waiting for accelerator calculations to complete. Then, in practical inference, we only need to update the complete instruction before the first model inference, and subsequent instruction updates will be hidden in the last model inference.

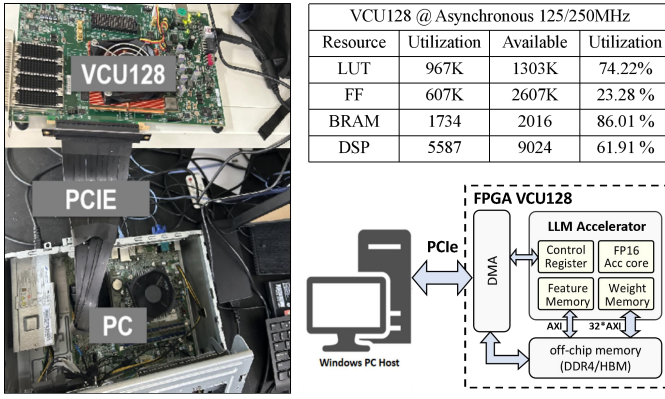


Fig. 13. Experimental setup for the CPU-FPGA heterogeneous system.

## VI. EXPERIMENTAL RESULTS

The proposed accelerator has been synthesized and implemented using Vivado 2023.1 on AMD Xilinx VCU128 board with 1303K logic elements (LUT), 2607K FF, 9024 DSP blocks, and 2016 Block RAMs on chip. Besides, the FPGA is equipped with 8GB HBM with 460GB/s bandwidth, which is well-suited for the acceleration of GB-level large language models.

Fig.13 shows the experimental setup for the system. The host computer (CPU) acts as the brain of the system, interfacing with the remaining components via the Peripheral Component Interconnect Express (PCIe) bus. It wields direct access privileges over DDR and HBM through the AXI-full protocol, enabling both read and write operations. Furthermore, it leverages the AXI lite protocol to interact with the accelerator IP's internal register array, thereby exercising control over the accelerator's operational dynamics. The proposed CPU-FPGA Heterogeneous accelerator contains four elements: CPU, HBM, DDR and Accelerator. Within the accelerator IP, all of the LLM operators have been meticulously incorporated, including matrix multiplication operator, multi-head attention mechanisms operator and so on. Among these, matrix multiplication operator, due to its extremely high demand for handling vast quantities of parameters, is connected with HBM in high frequency of 250MHz. While the other parts and operators work in 125MHz. The operation frequency can be further increased due to timing optimization.

Since the generation of tokens in the LLM is mainly in the Decode stage, and the Prefill stage only runs once, we mainly consider the generation speed of tokens in the Decode stage, which has been detailed shown in Table-III. The runtime of RMSNorm and FFN are independent to the Decode length, but the runtime of MHA has a quadratic relationship with the length. Specifically, the first decode delay is 14.15ms, corresponding peak speed about 75token/s, and the average speed for the first 128 tokens is about 67 token/s at a power of 50.77W, which shows  $1.67\times$  higher throughput and  $7.4\times$  higher energy efficiency than GPU [38].

TABLE III. Acceleration of ChatGLM on VCU128

VCU128 ChatGLM2	Operation	Input feature	weight	Output feature	MACs (GOP)	Delay (μs)
Block*28	RMSNorm	(1,4096)		(1,4096)	-	21.8
	MHA	MVM-BN (QK)	(1,4096) (4096, 4352)	(34,1,128)	0.035	26.04
		MVM-BN (V)	(1,4096) (4096, 256)	(2,1,128)	0.002	4.52
	Q head num=32	PosEmb (Q)	(32,1,128)	(32,1,128)	-	9.81
		PosEmb (K)	(2,1,128)	(2,1,128)	-	4.98
	KV head num=2	QK <sup>T</sup>	(32,1,128) (2,128,128)	(32,1,128)	0.135	13.92
		Softmax	(32,1,128)	(32,1,128)	-	40.19
	FFN	attn*V	(32,1,128) (2,128,128)	(1,4096)	0.134	13.78
		MVM-BN-Res	(1,4096) (4096, 4096)	(1,4096)	0.034	27.60
		RMSNorm	(1,4096)	(1,4096)	-	24.84
		MVM-BN	(1,4096) (4096, 13696)	(1,13696)	0.112	76.5
		SiLU (ACT)	(1,13696)	(1,13696)	-	32.22
		MVM-BN-Mul	(1,4096) (4096, 13696)	(1,13696)	0.112	77.09
		MVM-BN-Res	(1,13696) (13696, 4096)	(1,4096)	0.112	88.41
Output Layer	RMSNorm	(1,4096)	-	(1,4096)	-	19
	MVM-BN-MaxArg	(1,4096)	(4096, 65024)	(1,)	0.533	379.8
Summary	first_token_delay=13.33ms, <b>peak_speed=75.0token/s</b> , Decoding first 128token average_speed ~ 67token/s, <b>average_power=50.77W</b>					

Another important the efficiency of HBM in AI chips. Attaining high bandwidth utilization necessitates optimization at both the hardware and software levels. For instance, leveraging efficient dataflow architectures, optimizing memory access patterns, capitalizing on caching and re-utilization strategies. In our system, the HBM's bandwidth is 8192 bits per cycle. To full utilize this high bandwidth, we set the system to consume a corresponding 8192 bits of weight parameters per cycle, such good balance guarantees the high efficiency according to the roofline model [35]. The layer most intimately connected with maximizing bandwidth utilization is the matrix multiplication layer, namely the MVN-BN, MVM-BN-RES, or MVM-BN-MaxArg layer as shown in Table-III, which contains the optimization of operator fusion between MatMUL and BatchNorm or Shortcut or Argmax. In such layers, the HBM bandwidth ranges from 68% to 73.8%, which is higher than the competitor due to the elaborated dataflow design.

Fig.14 shows the total delay of MHA-stage and FFN-stage under different decoding token numbers. It can be seen that the runtime of RMSNorm and FFN are independent to the Decode length, but the runtime of MHA has a quadratic relationship with the length. When generating longer statements, the speed significantly slows down, which can be mitigated by applying on-chip quantization schemes and the strategy of locating the KV cache in HBM.



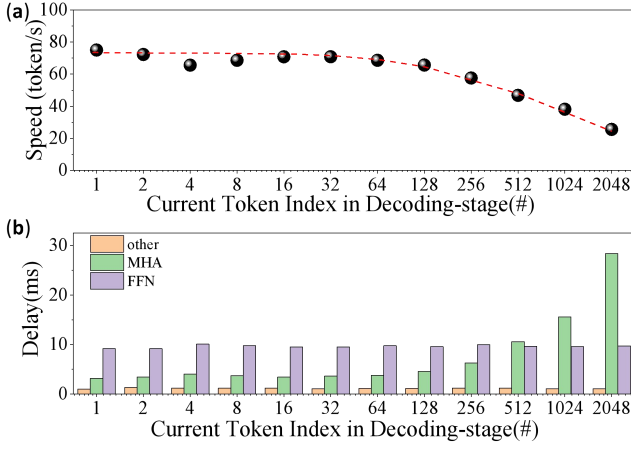


Fig. 14. Speed of the edgeLLM at different token index in decoding-stage.

TABLE IV. Comparison of Different Platform

Platform	A100 GPU	FlightLLM [1]		edgeLLM (this work)
		FPGA-U280	FPGA-VHK158	
Bandwidth Utilization	~30%	65.9%	64.8%	73.8%
Throughput	~45 token/s	~55token/s (on 7B LLM)	92.5 token/s (on 7B LLM)	~75 token/s (on 6B LLM)
Power	~220W	45W	155 W	50.77W
energy efficiency	0.2 token/J	1.22 token/J	0.6 token/J	1.47 token/J

Table IV shows the comparison of different platforms. GPU is widely used in LLMs. When accelerating large batch size data (typically for cloud scenarios), their performance and efficiency are very high. However, when the batch size is 1 (typically for edge application scenarios), the efficiency becomes typically lower than 30%. Besides, the energy consumption is also very high. FlightLLM [16] is currently state-of-the-art FPGA accelerator, enabling efficient LLMs inference with ~65% bandwidth utilization and 6 $\times$  better energy efficiency than GPU. Attributable to the synergistic effects of data format standardization, customized FP16\*INT4 operators, log-scale structured sparsity and asynchronous strategies, our integrated solution showcases enhanced performance over the FlightLLM by 11%-higher bandwidth utilization and 20%-higher energy efficiency, showing great potential for the practical edge-AI application.

## VII. CONCLUSION

This study proposes EdgeLLM, a high-performance CPU-FPGA heterogeneous acceleration scheme for the large language model. A multitude of optimization techniques have been integrated in the design. Firstly, we devise a unified and universal data format for the operator structures within AI algorithms, enabling the system to execute the entire sequence of operators swiftly and without interruption. Secondly, we have custom-designed dedicated FP16\*INT4 and FP16\*FP16 computational units with about 2 $\times$  higher efficiency than the

classical design. Besides, we develop approximate computation, group-vector systolic array and log-scale structured-sparsity computing engine to further boost the performance. Lastly, we propose end-to-end compilation scheme that can dynamically compile all of the operators and map the whole model. The accelerator has been successfully deployed on AMD Xilinx VCU128 FPGA platform. Our result achieves 1.67 $\times$  higher throughput and 7.4 $\times$  higher energy efficiency than GPU NVIDIA A100-SXM4-80G, and shows 10%~20% higher performance than state-of-the-art FPGA accelerator of FlightLLM.

## REFERENCES

- [1] Silver, David, et al. "Mastering the game of Go with deep neural networks and tree search." *Nature* 529.7587 (2016): 484-489.
- [2] Simonyan, Karen, and Andrew Zisserman. "Very deep convolutional networks for large-scale image recognition." *arXiv preprint arXiv:1409.1556* (2014).
- [3] K. He, X. Zhang, S. Ren, and J. Sun, "Deep residual learning for image recognition," in *Proceedings of the IEEE conference on computer vision and pattern recognition*, 2016, pp. 770-778.
- [4] Vaswani, Ashish, et al. "Attention is all you need." *Advances in neural information processing systems* 30 (2017).
- [5] Devlin, Jacob, et al. "Bert: Pre-training of deep bidirectional Transformers for language understanding." *arXiv preprint arXiv:1810.04805* (2018).
- [6] Dosovitskiy, Alexey, et al. "An image is worth 16x16 words: Transformers for image recognition at scale." *arXiv preprint arXiv:2010.11929* (2020).
- [7] Deng, Jia, et al. "Imagenet: A large-scale hierarchical image database." 2009 IEEE conference on computer vision and pattern recognition. IEEE CVPR, 2009.
- [8] LIN, Tsung-Yi, et al. Microsoft coco: Common objects in context. In: *Computer Vision – ECCV 2014: 13th European Conference, Zurich, Switzerland, September 6-12, 2014, Proceedings, Part V 13*. Springer International Publishing, 2014. p. 740-755.
- [9] Rishi Bommasani, Drew A Hudson, Ehsan Adeli, Russ Altman, Simran Arora, Sydney von Arx, Michael S Bernstein, Jeannette Bohg, Antoine Bosselut, Emma Brunskill, et al. 2021. On the opportunities and risks of foundation models. *arXiv preprint arXiv:2108.07258* (2021).
- [10] KASNECI, Enkelejda, et al. ChatGPT for good? On opportunities and challenges of large language models for education. *Learning and individual differences*, 2023, 103: 102274.
- [11] OpenAI. 2023. <https://chat.openai.com.chat> (2023)
- [12] Aakanksha Chowdhery, Sharan Narang, Jacob Devlin, Maarten Bosma, Gaurav Mishra, Adam Roberts, Paul Barham, Hyung Won Chung, Charles Sutton, Sebastian Gehrmann, et al. 2022. PaLM: Scaling language modeling with pathways. *arXiv preprint arXiv:2204.02311* (2022).
- [13] Thirunavukarasu, A. J., Ting, D. S. J., Elangovan, K., Gutierrez, L., Tan, T. F., & Ting, D. S. W. (2023). Large language models in medicine. *Nature medicine*, 29(8), 1930-1940.
- [14] ZHAO, Wayne Xin, et al. A survey of large language models. *arXiv preprint arXiv:2303.18223*, 2023.
- [15] DEMSZKY, Dorottya, et al. Using large language models in psychology. *Nature Reviews Psychology*, 2023, 2.11: 688-701.
- [16] Zeng, Shulin, et al. "Flightllm: Efficient large language model inference with a complete mapping flow on fpgas." *Proceedings of the 2024 ACM/SIGDA International Symposium on Field Programmable Gate Arrays*. 2024.
- [17] Li, Zhikai, and Qingyi Gu. "I-ViT: integer-only quantization for efficient vision transformer inference." *arXiv preprint arXiv:2207.01405* (2022).

- [18] Li B, Pandey S, Fang H, et al. "Ftrans: energy-efficient acceleration of Transformers using FPGA" Proceedings of the ACM/IEEE International Symposium on Low Power Electronics and Design. 2020: 175-180.
- [19] M. Huang et al., "A High Performance Multi-Bit-Width Booth Vector Systolic Accelerator for NAS Optimized Deep Learning Neural Networks," in IEEE Transactions on Circuits and Systems I: Regular Papers, vol. 69, no. 9, pp. 3619-3631, Sept. 2022, doi: 10.1109/TCSI.2022.3178474.
- [20] M. Huang et al. "An Integer-Only and Group-Vector Systolic Accelerator for Efficiently Mapping Vision Transformer on Edge. IEEE Transactions on Circuits and Systems I: Regular Papers", vol.70, no.12, pp. 5289 - 5301, 2023
- [21] Frantar, E., Ashkboos, S., Hoefler, T., & Alistarh, D. (2022). Gptq: Accurate post-training quantization for generative pre-trained transformers. arXiv preprint arXiv:2210.17323.
- [22] LIN, Ji, et al. AWQ: Activation-aware Weight Quantization for On-Device LLM Compression and Acceleration. Proceedings of Machine Learning and Systems, 2024, 6: 87-100.
- [23] LIU, Zichang, et al. Deja vu: Contextual sparsity for efficient llms at inference time. In: International Conference on Machine Learning. PMLR, 2023. p. 22137-22176.
- [24] FRANTAR, Elias; ALISTARH, Dan. Sparsegpt: Massive language models can be accurately pruned in one-shot. In: International Conference on Machine Learning. PMLR, 2023. p. 10323-10337.
- [25] LIU, Zichang, et al. Scissorhands: Exploiting the persistence of importance hypothesis for llm kv cache compression at test time. Advances in Neural Information Processing Systems, 2024, 36.
- [26] RAFFEL, Colin, et al. Exploring the limits of transfer learning with a unified text-to-text transformer. Journal of machine learning research, 2020, 21.140: 1-67.
- [27] XUE, Linting, et al. mT5: A massively multilingual pre-trained text-to-text transformer. arXiv preprint arXiv:2010.11934, 2020.
- [28] GLM, T., Zeng, A., Xu, B., Wang, B., Zhang, C., Yin, D., ... & Wang, Z. (2024). ChatGLM: A Family of Large Language Models from GLM-130B to GLM-4 All Tools. arXiv preprint arXiv:2406.12793.
- [29] ANIL, Rohan, et al. Palm 2 technical report. arXiv preprint arXiv:2305.10403, 2023.
- [30] OpenAI, "Sora: Creating video from text." <https://openai.com/sora>, 2024.
- [31] JOUPPI, Norman P., et al. In-datacenter performance analysis of a tensor processing unit. In: Proceedings of the 44th annual international symposium on computer architecture. 2017. p. 1-12.
- [32] JOUPPI, Norm, et al. Tpu v4: An optically reconfigurable supercomputer for machine learning with hardware support for embeddings. In: Proceedings of the 50th Annual International Symposium on Computer Architecture. 2023. p. 1-14.
- [33] Peng, Hongwu, et al. "Accelerating Transformer-based deep learning models on FPGA using column balanced block pruning." 2021 22nd International Symposium on Quality Electronic Design (ISQED). IEEE, 2021.
- [34] Wang, Teng, et al. "Via: A novel vision-Transformer accelerator based on FPGA." IEEE Transactions on Computer-Aided Design of Integrated Circuits and Systems 41.11 (2022): 4088-4099.
- [35] ZHANG, Chen, et al. Optimizing FPGA-based accelerator design for deep convolutional neural networks. In: Proceedings of the 2015 ACM/SIGDA international symposium on field-programmable gate arrays. 2015. p. 161-170.
- [36] Z. Liu, et al., " S2TA: Exploiting Structured Sparsity for Energy-Efficient Mobile CNN Acceleration," HPCA, 2022.
- [37] "NVIDIA A100 Tensor Core GPU Architecture," NVIDIA White-paper.
- [38] <https://github.com/THUDM/ChatGLM2-6B>.